Computational Techniques for Modeling Non-Newtonian Flow in Porous Media

Taha Sochi[*]

2010

[*]University College London, Department of Physics & Astronomy, Gower Street, London, WC1E 6BT. Email: t.sochi@ucl.ac.uk.

Contents

List of Figures

List of Tables

Abstract

Modeling the flow of Non-Newtonian fluids in porous media is a challenging subject. Several approaches have been proposed to tackle this problem. These include continuum models, numerical methods, and pore-scale network modeling. The latter proved to be more successful and realistic than the rest. The reason is that it captures the essential features of the flow and porous media using modest computational resources and viable modeling strategies. In this article we present pore-scale network modeling techniques for simulating non-Newtonian flow in porous media. These techniques are partially validated by theoretical analysis and comparison to experimental data.

1   Introduction

The flow of non-Newtonian fluids in porous media is highly important subject and has many applications as these fluids are the rule rather than the exception. These applications include filtration of polymer solutions, enhanced recovery from oil reservoirs, medical and biological technologies, and soil remediation by removing toxic substances. Newtonian fluids are those fluids exhibiting a direct proportionality between stress and strain rate in laminar flow. All fluids for which this proportionality is violated, due to nonlinearity or initial yield-stress, are said to be non-Newtonian. These fluids are commonly divided into three broad groups: time-independent in which strain rate solely depends on the instantaneous stress, time-dependent in which strain rate is a function of both magnitude and duration of the applied stress, and viscoelastic which shows partial elastic recovery on removal of the deforming stress. A large number of models have been proposed in the literature to model the bulk rheology of non-Newtonian fluids under various flow conditions. A range of modeling strategies and computational techniques have also been developed to depict the flow of these fluids in porous media. In this article we highlight the computational techniques that have been developed and implemented in our non-Newtonian code using network modeling approach.

In the context of fluid flow, 'porous medium' can be defined as a solid matrix through which small interconnected cavities occupying a measurable fraction of its volume are distributed. These cavities are of two types: large ones, called pores and throats, which contribute to the bulk flow of fluid; and small ones, comparable to the size of the molecules, which do not have an impact on the bulk flow though they may participate in other transportation phenomena like diffusion. The mathematical description of the flow in porous media is extremely complex and involves many approximations. In this regard, various methodologies have

been proposed and used. These include the continuum models, numerical methods and pore-scale network modeling. In this article we focus on network modeling as it is the methodology that we adopted in our flow simulation techniques.

Pore-scale network modeling is a relatively novel method developed to deal with the flow through porous media and other related issues. It can be seen as a compromise between the two extremes of continuum and numerical approaches as it partly accounts for the physics of flow and void space structure at pore level using affordable computational resources. Network modeling can be used to describe a wide range of properties from capillary pressure characteristics to interfacial area and mass transfer coefficients. The void space is described as a network of flow channels with idealized geometry. Rules that determine the transport properties in these channels are incorporated in the network to compute effective properties on a mesoscopic scale. The appropriate pore-scale physics combined with a representative description of the pore space gives models that can successfully predict average behavior [4, 5].

The general feature of network modeling is the representation of pore space by a network of interconnected ducts (bonds or throats) of regular shape and the use of a simplified form of the flow equations to describe the flow through the network. A numerical solver is normally employed to solve a system of simultaneous equations to determine the flow field. The network can be two-dimensional or three-dimensional with a random or regular lattice structure such as cubic. The shape of the cylindrical ducts include circular, square and triangular cross section and may include converging-diverging feature. The network elements may contain, beside the conducting ducts, nodes (pores) that can have zero or finite volume and may well serve a function in the flow phenomena or used as junctions to connect the bonds. The simulated flow can be Newtonian or non-Newtonian, single-phase, two-phase or even three-phase. The physical properties of the flow and porous

medium that can be obtained from flow simulation include absolute and relative permeability, formation factor, resistivity index, volumetric flow rate, apparent viscosity, threshold yield pressure and much more. Typical size of the network is a few millimeters. One reason for this minute size is to reduce the computational cost. Another reason is that this size is sufficient to represent a homogeneous medium having an average throat size of the most common porous materials. Up-scaling the size of a network is a trivial task if larger pore size is required. Moreover, extending the size of a network model by attaching identical copies of the same model in any direction or imposing repeated boundary conditions is another simple task.

The general strategy in network modeling is to use the bulk rheology of the fluid and the void space description of the porous medium as an input to the model. The flow simulation in a network starts by modeling the flow in a single capillary. For a network of capillaries, a set of equations representing the capillaries and satisfying mass conservation have to be solved simultaneously to find the pressure field and other physical quantities. For a network with n nodes there are n equations in n unknowns. These unknowns are the pressure values at the nodes. The essence of these equations is the continuity of flow of incompressible fluid at each node in the absence of sources and sinks. To find the pressure field, this set of equations have to be solved subject to the boundary conditions which are the pressures at the inlet and outlet of the network. This unique solution is 'consistent' and 'stable' as it is the only mathematically acceptable solution to the problem, and, assuming the modeling process and the mathematical technicalities are reliable, should mimic the unique physical reality of the pressure field in the porous medium. For Newtonian fluid, a single iteration is needed to solve the pressure field as the flow conductance is known in advance because the viscosity is constant. For purely viscous non-Newtonian fluid, the process starts with an initial guess for the viscosity, as it is

unknown and pressure-dependent, followed by solving the pressure field iteratively and updating the viscosity after each iteration cycle until convergence is reached. For memory fluids, the dependence on time must be taken into account when solving the pressure field iteratively.

2 Modeling the Flow in Porous Media

In our model we use three-dimensional networks built from a topologically-equivalent three-dimensional voxel image of the pore space with the pore sizes, shapes and connectivity reflecting the real medium. Pores and throats are modeled as having triangular, square or circular cross-section by assigning a shape factor which is the ratio of the area to the perimeter squared and obtained from the pore space image. Most of the network elements are not circular. To account for the non-circularity when calculating the volumetric flow rate analytically or numerically for a cylindrical capillary, an equivalent radius R_{eq} is defined

$$R_{eq} = \left(\frac{8G}{\pi}\right)^{1/4} \tag{1}$$

where G is the geometric conductance which may be obtained empirically from numerical simulation. The network can be extracted from voxel images of real porous materials or from voxel images generated by simulating the geological processes by which the porous medium was formed. Examples for the latter are the two networks of Statoil which represent two different porous media: a sand pack and a Berea sandstone. These networks are constructed by Øren and coworkers [6, 7] and have been used by several researchers in flow simulation studies. Another possibility for generating a network is by employing computational algorithms based on numeric statistical data extracted from the porous medium of interest. Other possibilities can also be found in the literature. An important aspect that characterizes the flow in porous media and makes it distinct from bulk is the presence of converging-diverging flow paths. This geometric factor significantly affects the flow and accentuates elastic responses. Therefore, a converging-diverging feature is introduced to the network capillaries when modeling viscoelastic flow.

Assuming a laminar, isothermal and incompressible flow at low Reynolds num-

ber, the only equations that require attention are the constitutive equation for the particular fluid and the conservation of volume as an expression for the conservation of mass. For Newtonian flow, the pressure field can be solved once and for all. For non-Newtonian flow, the situation is more complex as it involves non-linearities and requires iterative techniques. For the simplest case of time-independent fluids, the strategy is to start with an arbitrary guess. Because initially the pressure drop across each network element is not known, an iterative method is used. This starts by assigning an effective viscosity to the fluid in each element. The effective viscosity is defined as that viscosity which makes Poiseuille's equation fits any set of laminar flow conditions for time-independent fluids [8]. By invoking the conservation of volume for incompressible fluid, the pressure field across the entire network is solved using a numerical solver [9]. Knowing the pressure drops in the network, the effective viscosity of the fluid in each element is updated using the expression for the flow rate in a capillary with the Poiseuille's law as a definition. The pressure field is then recomputed using the updated viscosities and the iteration continues until convergence is achieved when a specified error tolerance in the total flow rate between two consecutive iteration cycles is reached. Finally, the total volumetric flow rate and the apparent viscosity, defined as the viscosity calculated from the Darcy's law, are obtained. Other physical parameters of interest that characterize the fluid and the porous medium may also be computed in this process.

3 Modeling Time-Independent Flow

Three time-independent fluids have been incorporated in the non-Newtonian model. These are Carreau, Ellis and Herschel-Bulkley. Carreau is a four-parameter model given by

$$\mu = \mu_\infty + \frac{\mu_o - \mu_\infty}{\left[1 + (\frac{\dot{\gamma}}{\dot{\gamma}_{cr}})^2\right]^{\frac{1-n}{2}}} \tag{2}$$

where μ is the fluid viscosity, μ_∞ is the viscosity at infinite shear, μ_o is the viscosity at zero shear, $\dot{\gamma}$ is the shear rate, n is the flow behavior index, and $\dot{\gamma}_{cr}$ is a critical shear rate given by

$$\dot{\gamma}_{cr} = \left(\frac{\mu_o}{C}\right)^{\frac{1}{n-1}} \tag{3}$$

where C is the consistency factor of the equivalent shear-thinning fluid in the power-law formulation. This model was previously implemented and fully described by Lopez [10] and Lopez *et al* [11]. In summary, the implementation of Carreau model relies on the use of an empirical expression for the volumetric flow rate in a single tube. The reader should refer to those references for details.

Ellis is a three-parameter model which describes time-independent shear-thinning yield-free non-Newtonian fluids. It is used as a substitute for the power-law and is appreciably better than the power-law model in matching experimental measurements. Its distinctive feature is the low-shear Newtonian plateau without a high-shear plateau. According to this model, the fluid viscosity μ is given by [12–15]

$$\mu = \frac{\mu_o}{1 + \left|\dfrac{\tau}{\tau_{1/2}}\right|^{\alpha-1}} \tag{4}$$

where μ_o is the low-shear viscosity, τ is the shear stress, $\tau_{1/2}$ is the shear stress at which $\mu = \mu_o/2$ and α is a dimensionless indicial parameter related to the slope in the power-law region. For Ellis fluids, the volumetric flow rate in a circular cylindrical tube is given by [12–15]:

$$Q = \frac{\pi R^4 \Delta P}{8L\mu_o}\left[1 + \frac{4}{\alpha+3}\left(\frac{R\Delta P}{2L\tau_{1/2}}\right)^{\alpha-1}\right] \tag{5}$$

where R is the tube radius, ΔP is the pressure drop across the tube and L is the tube length.

Herschel-Bulkley is a three-parameter model that can describe Newtonian and a large group of time-independent non-Newtonian fluids. It is given by [8]

$$\tau = \tau_o + C\dot{\gamma}^n \qquad (\tau > \tau_o) \tag{6}$$

where τ is the shear stress, τ_o is the yield-stress above which the substance starts flowing, C is the consistency factor, $\dot{\gamma}$ is the shear rate and n is the flow behavior index. Herschel-Bulkley reduces to the power-law, or Ostwald-de Waele model, when the yield-stress is zero, to the Bingham plastic model when the flow behavior index is unity, and to the Newton's law for viscous fluids when both these conditions are met. For Herschel-Bulkley fluids, the volumetric flow rate in a cylindrical capillary at yield is given by [8]:

$$Q = \frac{8\pi}{C^{\frac{1}{n}}}\left(\frac{L}{\Delta P}\right)^3(\tau_w - \tau_o)^{1+\frac{1}{n}}\left[\frac{(\tau_w - \tau_o)^2}{3+1/n} + \frac{2\tau_o(\tau_w - \tau_o)}{2+1/n} + \frac{\tau_o^2}{1+1/n}\right]$$
$$(\tau_w > \tau_o) \tag{7}$$

where τ_w $(= \frac{\Delta P R}{2L})$ is the shear stress at the tube wall.

The implementation of Ellis and Herschel-Bulkley is based on the use of the analytical expressions for the volumetric flow rate in a circular cylindrical duct, as given above (i.e. Equation 5 for Ellis and Equation 7 for Herschel-Bulkley). These expressions are used in conjunction with an iterative technique to find the total flow across the network, as outlined in § 2.

4 Modeling Yield-Stress

Yield-stress or viscoplastic fluids can sustain shear stresses, that is a certain amount of stress must be exceeded before the flow starts. So an ideal yield-stress fluid is a solid before yield and a fluid after. Accordingly, the viscosity of the substance changes from an infinite to a finite value. However, the physical situation suggests that it is more realistic to regard a yield-stress substance as a fluid whose viscosity as a function of applied stress has a discontinuity as it drops sharply from a very high value on exceeding a critical stress. Several constitutive equations to describe yield-stress substances are in use; the most popular ones are Bingham, Casson and Herschel-Bulkley. In our network model, yield-stress was implemented within the Herschel-Bulkley fluid. A number of numerical algorithms, related to or independent of Herschel-Bulkley, were also implemented in the model.

The implementation of the yield-stress in a network is based on the yield condition for its conducting ducts which are assumed to be circular cylinders. The verification of the yield condition in the individual ducts associates the process of solving the pressure field in the network. For yield-stress fluids, the threshold pressure drop above which the flow in a single tube starts is given by

$$\Delta P_{th} = \frac{2L\tau_o}{R} \tag{8}$$

where ΔP_{th} is the threshold pressure drop, τ_o is the yield-stress and R and L are the tube radius and length respectively.

In our model, the substance before yield is considered to be fluid with very high but finite viscosity so the flow virtually vanishes. The reason is that the pressure across the network have to communicate. Accordingly, the pressure field in the case of yield-stress fluids is solved as in the case of non-yield-stress fluids. A further

condition is also imposed before any duct is allowed to yield, that is the duct must be part of a non-blocked path spanning the network from the inlet to the outlet. The logic is that any conducting duct should have a source on one side and a sink on the other.

4.1   Predicting Threshold Yield Pressure of a Network

Non-Newtonian literature contains several attempts to predict the yield point of a complex porous medium from the void space description and yield-stress value of an ideal yield-stress fluid without modeling the flow process. In this regard, there is an implicit assumption that the network is an exact replica of the medium and the yield-stress value reflects the real yield-stress of fluid so that any failure of these proposals can not be attributed to mismatch or any factor other than flaws in these proposals. Our discussion in this section will focus on the Invasion Percolation with Memory (IPM) and Path of Minimum Pressure (PMP) algorithms which are implemented in the network model to make such predictions.

The IPM is an algorithm for finding the inlet-to-outlet path that minimizes the sum of values of a property assigned to the individual elements of the network, and hence finding this minimum. For a yield-stress fluid, this reduces to finding the inlet-to-outlet path that minimizes the yield pressure. The yield pressure of this path is then taken as the network threshold yield pressure. A flow chart of the IPM algorithm is presented in Figure (1). The PMP algorithm is based on a similar assumption to that upon which the IPM is based, that is the network threshold yield pressure is the minimum sum of the threshold yield pressures of the individual elements of all possible paths from the inlet to the outlet. However, PMP is computationally different and is more efficient than the IPM in terms of the required computational resources (memory and CPU time). A flow chart

depicting the PMP algorithm is given in Figure (2). In most cases that have been investigated the IPM and PMP produce identical results.

Another algorithm, called Actual Threshold Pressure (ATP), for finding the network yield point by solving the pressure field was also developed and implemented. The ATP is an iterative simulation algorithm which uses the solver to find the network yield pressure to the required accuracy. However, this algorithm is not independent of Herschel-Bulkley model as it relies on multiple applications of flow simulation of this model.
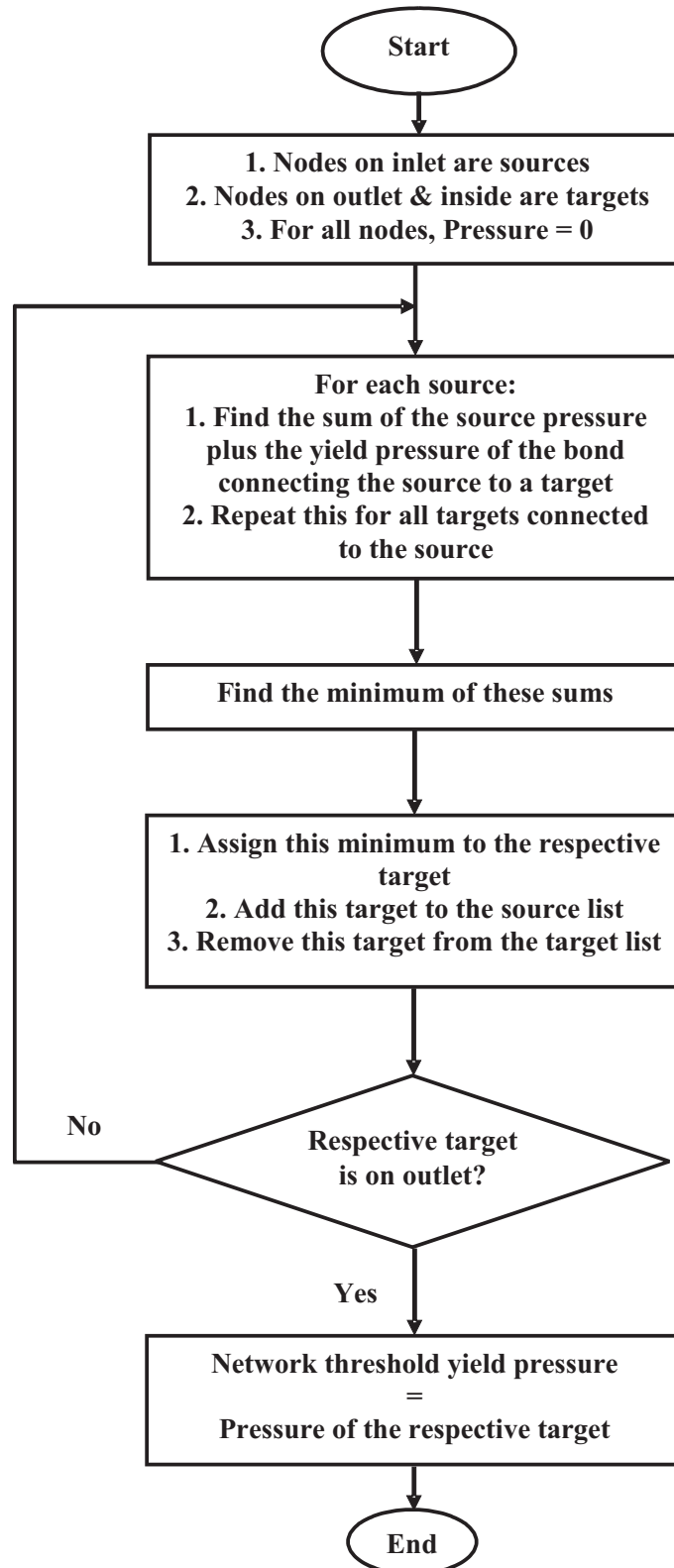
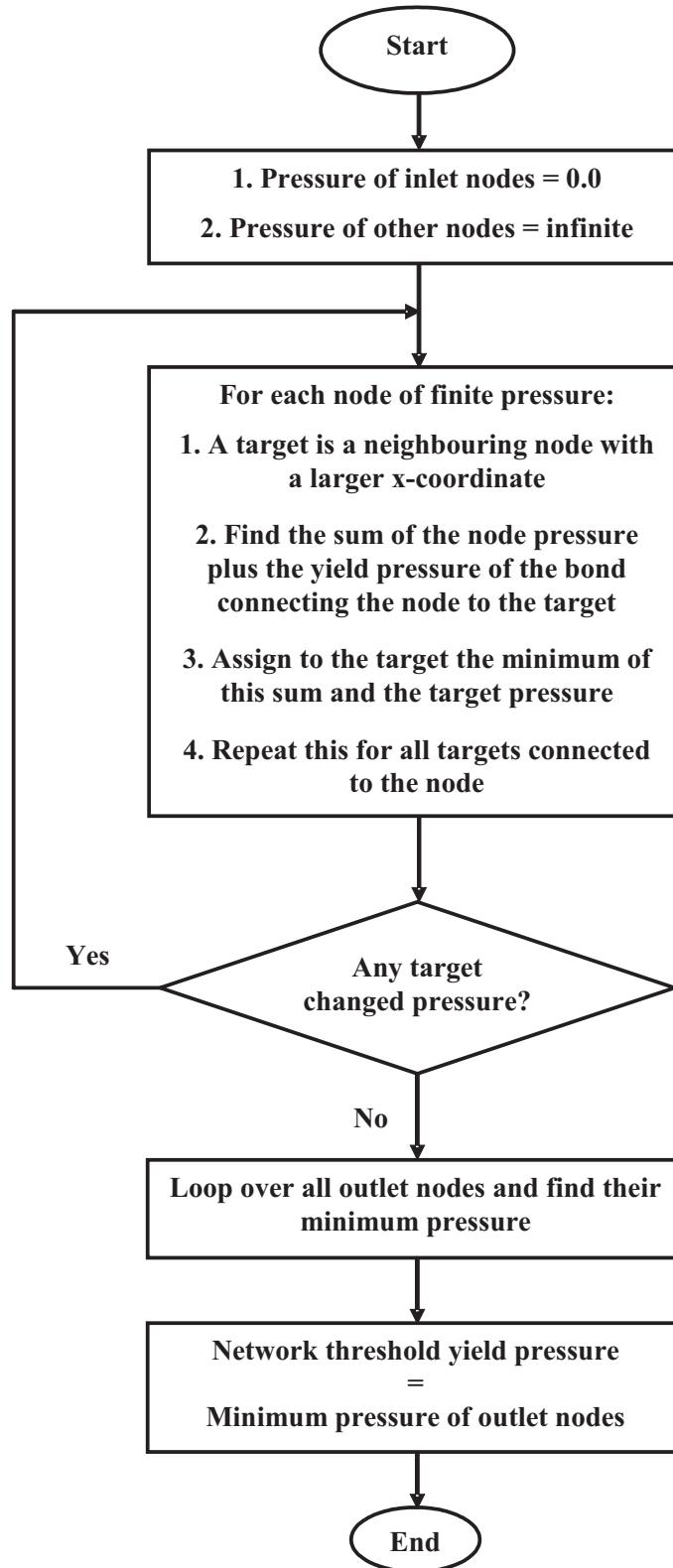Figure 1: Flowchart of the Invasion Percolation with Memory (IPM) algorithm.

Figure 2: Flowchart of the Path of Minimum Pressure (PMP) algorithm.

5 Modeling Time-Dependent Flow

In theory, time-dependence effects can arise from thixotropic (and rheopectic) structural change or from time-dependent viscoelasticity or from both effects simultaneously. The existence of these two different types of time-dependent rheological behavior is generally recognized. Although it is convenient to distinguish between these as two separate phenomena, real fluids can exhibit both types simultaneously. Several physical distinctions between viscoelastic and thixotropic time-dependence have been made. The important one is that while time-dependence of viscoelastic fluids arises from relaxation and delayed response, time-dependence of thixotropic fluids arises from structural change. With regards to modeling the flow in porous media of complex fluids that have time dependency in a dynamic sense due to thixotropic or elastic nature, there are three major difficulties

- The difficulty of tracking the fluid elements in the pores and throats and identifying their deformation history, as the path followed by these elements is random and can have several unpredictable outcomes.

- The mixing of fluid elements with various deformation history in the individual pores and throats. As a result, the viscosity is not a well-defined property of the fluid in the pores and throats.

- The change of viscosity along the streamline since the deformation history is continually changing over the path of each fluid element.

These complications have not been considered in the current model, and hence no dynamic time-dependence has been included in the code. However, general strategies for simulating time-dependent thixotropic behavior have been considered. These strategies can provide a framework for future development. There are three major cases of flow simulation of thixotropic fluids in porous media:

- The flow of strongly strain-dependent fluid in a porous medium which is not highly homogeneous. This case is very difficult to model due to the difficulty of tracking the fluid elements in the pores and throats and determining their deformation history. Moreover, the viscosity function may not be well defined due to the mixing of fluid elements with various deformation history in the individual pores and throats.

- The flow of strain-independent or weakly strain-dependent fluid through porous media in general. A possible strategy is to apply single time-dependent viscosity function to all pores and throats at each instant of time and hence simulating time development as a sequence of Newtonian states.

- The flow of strongly strain-dependent fluid in a highly homogeneous porous medium such that the fluid is subject to the same deformation in all ducts. The strategy for modeling this flow is to define an effective pore strain rate. Then using a very small time step the strain rate in the next instant of time can be found assuming constant strain rate. As the change in the strain rate is then known, a correction to the viscosity due to strain-dependency can be introduced.

It should be remarked that the Bautista-Manero fluid, which is used to model steady-state viscoelastic flow, incorporates thixotropic as well as viscoelastic attributes.

6 Modeling Viscoelastic Flow

As indicated already, no dynamic time-dependence has been included in the non-Newtonian flow model. For the steady-state flow of viscoelastic fluids, the approach of Tardy [16, 17] was used with some adaptation. In this approach, the capillaries of the network are modeled with contraction to account for the effect of converging-diverging geometry on the flow. The reason is that the effects of fluid memory take place on going through a radius change, as this change induces a change in strain rate with viscosity changing consequences. The capillaries are also discretized in the flow direction and a discretized form of the flow equations is used with assumed prior knowledge of the stress and viscosity at the inlet of the network. Starting with an initial guess for the flow rate and using iterative technique, the pressure drop as a function of the flow rate is then found in each capillary. Finally, the pressure field for the whole network is found iteratively until convergence is achieved. Once this happens, the flow rate through each capillary in the network can be computed and the total flow rate through the network is determined by summing and averaging the flow through the inlet and outlet capillaries.

This algorithm employs a one-dimensional version of the Bautista-Manero model which combines the Fredrickson kinetic equation for flow-induced structural changes with the Oldroyd-B constitutive equation for viscoelasticity. The model requires six parameters that have physical significance and can be estimated from rheological measurements. Bautista-Manero model was originally proposed for the rheology of worm-like micellar solutions which usually have an upper Newtonian plateau, and show strong signs of shear-thinning. The model, which incorporates shear-thinning, elasticity and thixotropy, can be used to describe the complex rheological behavior of viscoelastic systems that also exhibit thixotropy and rheopexy under shear flow [16, 18–20].

The kinetic equation of Fredrickson that accounts for the destruction and construction of structure is given by

$$\frac{\mathrm{d}\mu}{\mathrm{d}t} = \frac{\mu}{\lambda}\left(1 - \frac{\mu}{\mu_o}\right) + k\mu\left(1 - \frac{\mu}{\mu_\infty}\right)\boldsymbol{\tau} : \dot{\boldsymbol{\gamma}} \tag{9}$$

where μ is the viscosity, t is the time of deformation, λ is the relaxation time, μ_o and μ_∞ are the viscosities at zero and infinite shear rates respectively, k is a parameter that is related to a critical stress value below which the material exhibits primary creep, $\boldsymbol{\tau}$ is the stress tensor and $\dot{\boldsymbol{\gamma}}$ is the rate of strain tensor. In this model, λ is a structural relaxation time, whereas k is a kinetic constant for structure break down [16, 18–20].

The Oldroyd-B constitutive equation is given by [14]

$$\boldsymbol{\tau} + \lambda_1\overset{\triangledown}{\boldsymbol{\tau}} = \mu_o\left(\dot{\boldsymbol{\gamma}} + \lambda_2\overset{\triangledown}{\dot{\boldsymbol{\gamma}}}\right) \tag{10}$$

where λ_1 is the relaxation time, λ_2 is the retardation time, and $\overset{\triangledown}{\dot{\boldsymbol{\gamma}}}$ is the upper convected time derivative of the rate-of-strain tensor given by

$$\overset{\triangledown}{\dot{\boldsymbol{\gamma}}} = \frac{\partial\dot{\boldsymbol{\gamma}}}{\partial t} + \mathbf{v}\cdot\nabla\dot{\boldsymbol{\gamma}} - (\nabla\mathbf{v})^T\cdot\dot{\boldsymbol{\gamma}} - \dot{\boldsymbol{\gamma}}\cdot\nabla\mathbf{v} \tag{11}$$

Similar expression applies to the upper convected time derivative of the stress tensor $\overset{\triangledown}{\boldsymbol{\tau}}$. A flow chart outlining the steady-state viscoelastic flow simulation algorithm is presented in Figure (3).

Start

Model each capillary in the network
with converging-diverging geometry

Discretize each capillary into slices

For capillaries at the network inlet, assume initial values for viscosity
and stress at their inlet. For other capillaries, use Q-weighted averages

Obtain initial volumetric flow rate, average speed and shear
rate of fluid in each capillary assuming Newtonian flow

For each capillary, calculate viscosity and stress slice by
slice, where values from the previous slice are used to
obtain values for the current slice

Find the pressure drop across the slice using Poiseuille

Find the pressure drop across the capillary by adding the pressures of
individual slices and hence find the effective viscosity for the capillary

Solve the pressure field across the network, and hence
obtain the total flow rate and apparent viscosity

Obtain volumetric
flow rate, average
speed and shear
rate of fluid in
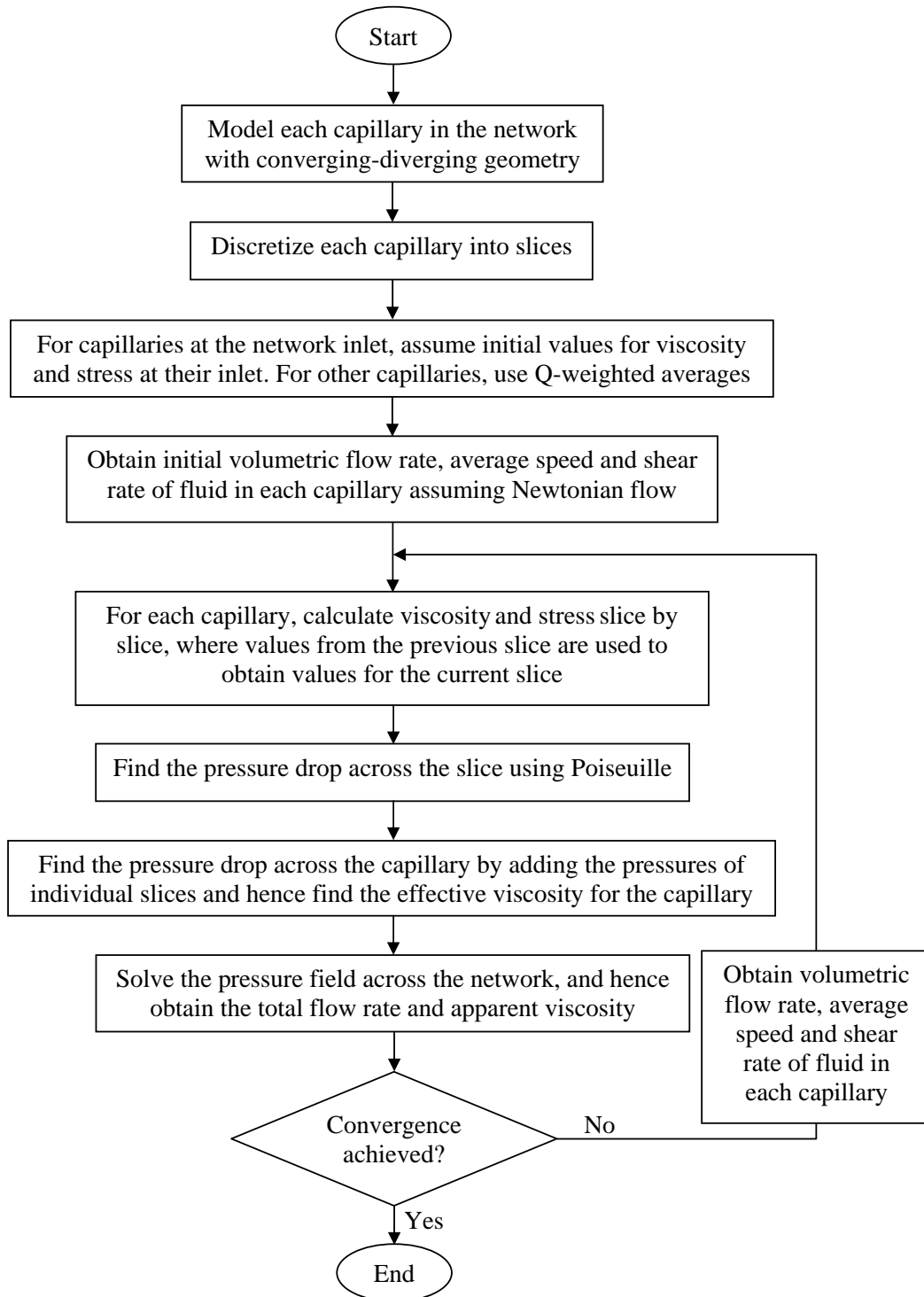each capillary

Convergence
achieved?

No

Yes

End

Figure 3: Flow chart of the steady-state viscoelastic flow simulation algorithm.

7   Validation and Results

These computational techniques as implemented in the non-Newtonian code were quantitatively validated in a number of cases. These include low flow rate regimes, Bingham fluids at high flow rates, Boger fluids, and Newtonian as a special case of non-Newtonian model [17, 21, 22]. Two randomly-distributed networks representing two different porous media, a sand pack and a Berea sandstone, were used in these validations. These networks are constructed by Øren and coworkers [6, 7] from voxel images generated by simulating the geological processes by which the porous medium was formed. The sand pack comprises 13490 elements (pores and throats) with a cube side length of 2.5mm, while the Berea consists of 38495 elements with a cube side of 3mm. The physical and statistical properties of these networks with detailed comparison between them can be found in [17, 21].

These computational techniques were also partially validated by a number of experimental data sets found in the literature for time-independent fluids [17, 21]. A sample of these data with their simulation counterparts are given in Figures (4), (5) and (6) for Ellis, Herschel-Bulkley and Bingham fluids respectively. The bulk rheologies of these data sets are presented in Tables (1), (2) and (3) respectively. In these simulations, scaled versions of the sand pack network were used. The purpose of scaling is to match the network characteristics to the characteristics of the corresponding porous media. The sand pack was used instead of Berea because it is a better match to the experimental packed beds in terms of homogeneity and tortuosity. The experimental validation is based on using the experimental bulk rheology and bed properties as an input to the non-Newtonian code. Qualitatively, all trends of behavior that have been observed are sensible. The major failure of the non-Newtonian model occurs in the case of fluids with yield-stress. Although the quality of some experimental data sets may be questionable, it seems that the

yield-stress model, which is based on the concept of equivalent radius of cylindrical capillaries, is too simplistic and unrealistic and hence is very unlikely to produce reliable predictions.
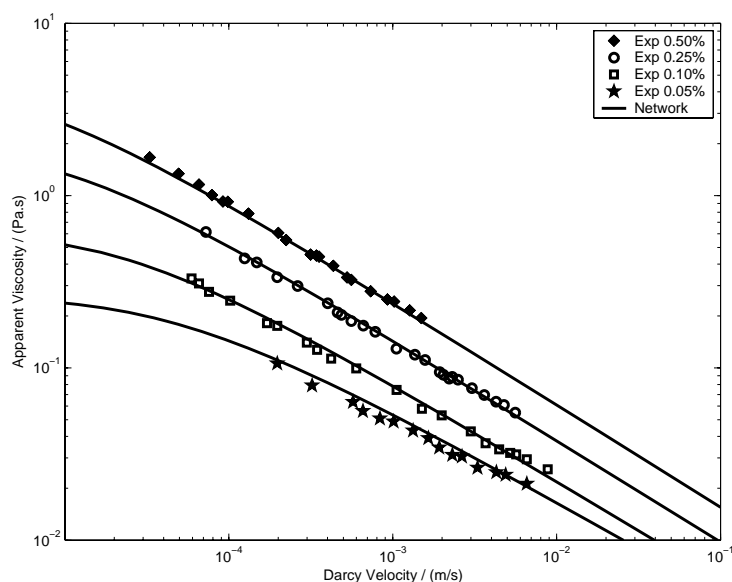

Figure 4: Park's Ellis experimental data sets [1] for polyacrylamide solutions with 0.50%, 0.25%, 0.10% and 0.05% weight concentration flowing through a coarse packed bed of glass beads having $K = 3413$ Darcy and $\phi = 0.42$ alongside the simulation results obtained with a scaled sand pack network having the same K presented on a log-log scale. The bulk rheology of these data is given in Table 1.
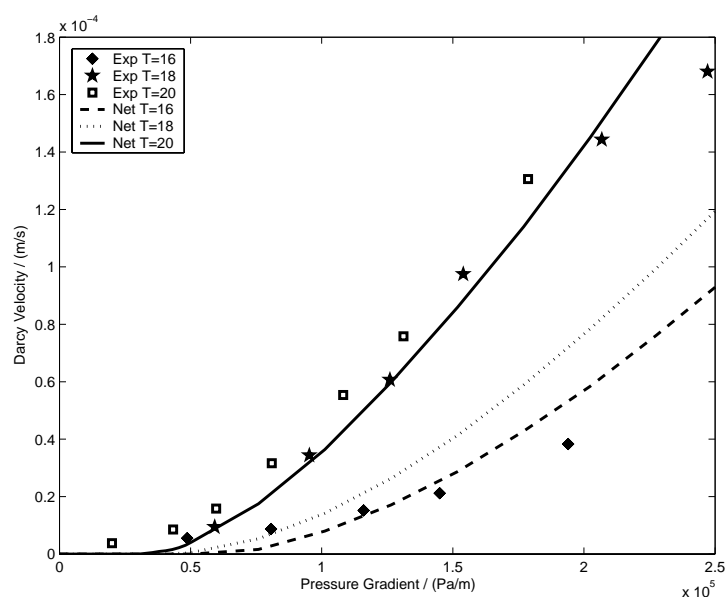
Figure 5: Al-Fariss and Pinder's Herschel-Bulkley experimental data sets [2] for 5.0% wax in Clarus B oil flowing through a column of sand having $K = 315$ Darcy and $\phi = 0.36$ alongside the simulation results obtained with a scaled sand pack network having the same K and ϕ. The temperatures, T, are in °C. The bulk rheology of these data is given in Table 2.
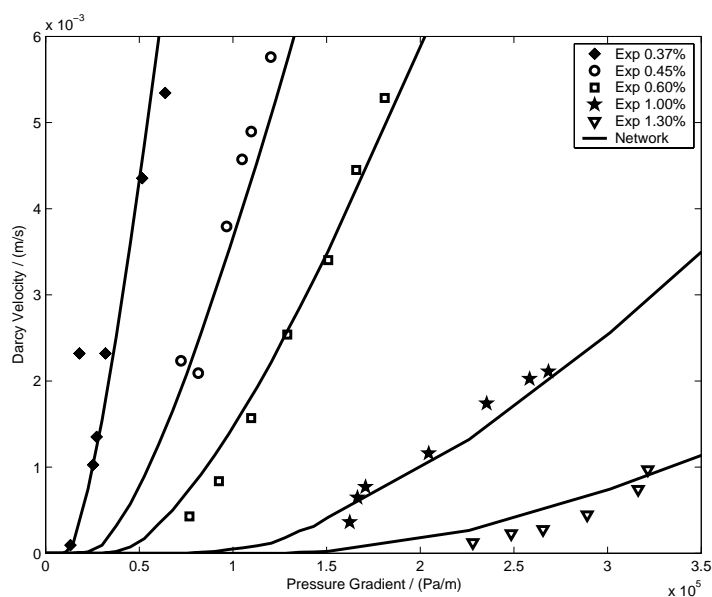

Figure 6: Network simulation results with the corresponding experimental data points of Chase and Dachavijit [3] for Bingham aqueous solutions of Carbopol 941 with various concentrations (0.37%, 0.45%, 0.60%, 1.00% and 1.30%) flowing through a packed column of glass beads. The bulk rheology of these data is given in Table 3.

Table 1: The bulk rheology of Park's Ellis experimental data sets [1].

Dataset	μ_o (Pa.s)	α	$\tau_{1/2}$ (Pa)
0.50%	4.35213	2.4712	0.7185
0.25%	1.87862	2.4367	0.5310
0.10%	0.60870	2.3481	0.3920
0.05%	0.26026	2.1902	0.3390

Table 2: The bulk rheology of Al-Fariss and Pinder's Herschel-Bulkley experimental data sets [2].

Dataset	C (Pa.s^n)	n	τ_o (Pa)
T=16	0.463	0.87	3.575
T=18	0.568	0.80	2.650
T=20	0.302	0.90	1.921

Table 3: The bulk rheology of Chase and Dachavijit's Bingham experimental data sets [3].

Dataset	C (Pa.s^n)	n	τ_o (Pa)
0.37%	0.017	1.0	2.06
0.45%	0.038	1.0	4.41
0.60%	0.057	1.0	7.09
1.00%	0.128	1.0	17.33
1.30%	0.215	1.0	28.46

8 Non-Newtonian Code

The computer code in which these computational techniques have been implemented is derived from the non-Newtonian code of Lopez [10] which was constructed from an early version of the Newtonian code by Valvatne [23]. Beside the Carreau model, which is inherited from the original code of Lopez, the current code can simulate the flow of Ellis and Herschel-Bulkley fluids. Several algorithms related to yield-stress and a modified version of the Tardy algorithm to simulate steady-state viscoelastic flow using the Bautista-Manero model are also implemented. The code can be downloaded from this URL: http://www3.imperial.ac.uk/earthscienceandengineering/research/perm/porescalemodelling/software/non-newtonian%20code or this URL: www.scienceware.net/id2.html.

The code has a command line interface that uses a keyword-based input file. Convergence time generally depends on the fluid rheology, the size of network and the type of algorithm. A typical convergence time for the sand pack and Berea sandstone networks used in this study is a second for the time-independent models and a few seconds for the viscoelastic model. The time requirement for the yield-stress algorithms is highly dependent on the last two factors. However, there is significant difference between the IPM and PMP convergence time. As these two algorithms produce very similar results, it is recommended to use the PMP for large networks. In all cases, the memory requirement does not exceed a few tens of megabytes for a network with up to 12000 pores. In general, the memory cost is affordable on a typical modern workstation for all available networks. The general flow sequence of the program is as follows:

- The program starts by reading the input and network data files followed by creating the network.

- For fluids with yield-stress, the program executes IPM and PMP algorithms

to predict the threshold yield pressure of the network. This is followed by an iterative simulation algorithm to find the network actual threshold yield pressure to the required accuracy.

- Single-phase flow of a Newtonian fluid is simulated to find the fluid-related network properties such as absolute permeability.

- Single-phase flow of Newtonian and non-Newtonian fluids is simulated for a range of pressure points as defined by the user.

In all stages, informative messages are issued about the program progress and the data obtained. The program also creates several output data files. These include script files to visualize the entire network or slice of it and the flow path of yield-stress fluid using Rhino 3D program.

9 Conclusions and Discussions

In this study, we outlined a set of computational techniques based on pore-scale network modeling to simulate single-phase flow of non-Newtonian fluids in porous media. These techniques are implemented in a computer code and have been partially validated analytically and experimentally.

1. The success was evident in the case of time-independent fluids. This includes comparison with a number of experimental data sets and correct predictions in special and limiting cases such as Newtonian fluids and the asymptotic behavior of Bingham at high flow rates.

2. Steady-state viscoelastic flow simulation has also produced reliable results in the case of low flow rate regimes and Boger fluids. Moreover, qualitatively sensible trends of behavior were observed in the other cases using several parameters related to the fluid, porous media and numerical indicators.

3. Thixotropic flow as such has not been modeled although thixotropic aspects are included within the Bautista-Manero model which is the basis of the steady-state viscoelastic flow algorithm. However, thixotropic computational strategies have been developed and assessed.

4. The predictions were less satisfactory in the case of yield-stress fluids. This may be explained by inadequate representation of the pore space structure, experimental errors and involvement of other physical phenomena. Minimum threshold path algorithms (i.e. IPM and PMP) have also been developed and implemented. The analysis revealed that these algorithms are too simplistic and hence cannot produce reliable predictions for the pressure yield point of a network.

Nomenclature

α	parameter in Ellis model
$\dot{\gamma}$	strain rate (s^{-1})
$\dot{\gamma}_{cr}$	critical shear rate (s^{-1})
$\dot{\boldsymbol{\gamma}}$	rate-of-strain tensor
λ	structural relaxation time in Fredrickson model (s)
λ_1	relaxation time (s)
λ_2	retardation time (s)
μ	viscosity (Pa.s)
μ_o	zero-shear viscosity (Pa.s)
μ_∞	infinite-shear viscosity (Pa.s)
τ	stress (Pa)
$\boldsymbol{\tau}$	stress tensor
$\tau_{1/2}$	stress when $\mu = \mu_o/2$ in Ellis model (Pa)
τ_o	yield-stress (Pa)
τ_w	stress at tube wall (Pa)
ϕ	porosity
C	consistency factor (Pa.s^n)
G	geometric conductance (m^4)
G'	flow conductance ($\text{m}^3.\text{Pa}^{-1}.\text{s}^{-1}$)
k	parameter in Fredrickson model (Pa^{-1})
K	absolute permeability
L	tube length (m)

n	flow behavior index
P	pressure (Pa)
ΔP	pressure drop (Pa)
ΔP_{th}	threshold pressure drop (Pa)
Q	volumetric flow rate (m^3.s^{-1})
R	tube radius (m)
R_{eq}	equivalent radius (m)
t	time (s)
T	temperature (K, °C)
v	fluid velocity vector

ATP	Actual Threshold Pressure algorithm
IPM	Invasion Percolation with Memory algorithm
PMP	Path of Minimum Pressure algorithm
$\overset{\triangledown}{\cdot}$	upper convected time derivative
$(\cdot)^T$	matrix transpose

Note: units, when relevant, are given in the SI system. Vectors and tensors are marked with boldface. Some symbols may rely on the context for unambiguous identification.

References

[1] H.C. Park. *The flow of non-Newtonian fluids through porous media*. PhD thesis, Michigan State University, 1972.

[2] T.F. Al-Fariss; K.L. Pinder. Flow of a shear-thinning liquid with yield stress through porous media. *SPE 13840*, 1984.

[3] G.G. Chase; P. Dachavijit. Incompressible cake filtration of a yield stress fluid. *Separation Science and Technology*, 38(4):745–766, 2003.

[4] M.J. Blunt. Flow in porous media - pore-network models and multiphase flow. *Colloid and Interface Science*, 6(3):197–207, 2001.

[5] M.J. Blunt; M.D. Jackson; M. Piri; P.H. Valvatne. Detailed physics, predictive capabilities and macroscopic consequences for pore-network models of multiphase flow. *Advances in Water Resources*, 25:1069–1089, 2002.

[6] P.E. Øren; S. Bakke; O.J. Amtzen. Extending predictive capabilities to network models. *SPE Annual Technical Conference and Exhibition, San Antonio, Texas*, (SPE 38880), 1997.

[7] P.E. Øren; S. Bakke. Reconstruction of berea sandstone and pore-scale modelling of wettability effects. *Journal of Petroleum Science and Engineering*, 39:177–199, 2003.

[8] A.H.P. Skelland. *Non-Newtonian Flow and Heat Transfer*. John Wiley and Sons Inc., 1967.

[9] J.W. Ruge; K. Stüben. *Multigrid Methods: Chapter 4 (Algebraic Multigrid), Frontiers in Applied Mathematics*. SIAM, 1987.

[10] X. Lopez. *Pore-scale modelling of non-Newtonian flow*. PhD thesis, Imperial College London, 2004.

[11] X. Lopez; P.H. Valvatne; M.J. Blunt. Predictive network modeling of single-phase non-Newtonian flow in porous media. *Journal of Colloid and Interface Science*, 264:256–265, 2003.

[12] T.J. Sadowski; R.B. Bird. Non-Newtonian flow through porous media I. Theoretical. *Transactions of the Society of Rheology*, 9(2):243–250, 1965.

[13] J.G. Savins. Non-Newtonian flow through porous media. *Industrial and Engineering Chemistry*, 61(10):18–47, 1969.

[14] R.B. Bird; R.C. Armstrong; O. Hassager. *Dynamics of Polymeric Liquids*, volume 1. John Wily & Sons, second edition, 1987.

[15] P.J. Carreau; D. De Kee; R.P. Chhabra. *Rheology of Polymeric Systems*. Hanser Publishers, 1997.

[16] P. Tardy; V.J. Anderson. Current modelling of flow through porous media. *Private communication*, 2005.

[17] T. Sochi. *Pore-Scale Modeling of Non-Newtonian Flow in Porous Media*. PhD thesis, Imperial College London, 2007.

[18] F. Bautista; J.F.A. Soltero; J.H. Pérez-López; J.E. Puig; O. Manero. On the shear banding flow of elongated micellar solutions. *Journal of Non-Newtonian Fluid Mechanics*, 94(1):57–66, 2000.

[19] F. Bautista; J.M. de Santos; J.E. Puig; O. Manero. Understanding thixotropic and antithixotropic behavior of viscoelastic micellar solutions and liquid crystalline dispersions. I. The model. *Journal of Non-Newtonian Fluid Mechanics*, 80(2):93–113, 1999.

[20] O. Manero; F. Bautista; J.F.A. Soltero; J.E. Puig. Dynamics of worm-like

micelles: the Cox-Merz rule. *Journal of Non-Newtonian Fluid Mechanics*, 106(1):1–15, 2002.

[21] T. Sochi; M.J. Blunt. Pore-scale network modeling of Ellis and Herschel-Bulkley fluids. *Journal of Petroleum Science and Engineering*, 60(2):105–124, 2008.

[22] T. Sochi. Pore-scale modeling of viscoelastic flow in porous media using a Bautista-Manero fluid. *International Journal of Heat and Fluid Flow*, 30(6):1202–1217, 2009.

[23] P.H. Valvatne. *Predictive pore-scale modelling of multiphase flow*. PhD thesis, Imperial College London, 2004.